Mechanistic Insights on Cytotoxicity of KOLR by targeting Signaling Complexes of phosphodiesterase 3B and Rap guanine nucleotide exchange factor 3

Mingqian Li
Tongde Hospital Of Zhejiang Province https://orcid.org/0000-0002-3296-6868
Fei Li
Sichuan Normal University
Jiabin Chen
Tongde Hospital Of Zhejiang Province
Guanping Chen
Tongde Hospital Of Zhejiang Province
Jili Cao
Tongde Hospital Of Zhejiang Province
Jiacheng Li
Sichuan Normal University
Liyao Dong
Sichuan Normal University
Zhihong Yu
Tongde Hospital Of Zhejiang Province
Yifan Wang
Tongde Hospital Of Zhejiang Province
Jing Li
Tongde Hospital Of Zhejiang Province
Yingyan Lu
Tongde Hospital Of Zhejiang Province
Chun Zhou
People's Liberation Army Joint Logistic Support Force 903th Hospital
Yongqiang Zhu
Tongde Hospital Of Zhejiang Province
Qun Li
Sichuan Normal University
Kequn Chai (ckq_official@163.com)
Tongde Hospital of Zhejiang Province

Research

Keywords: Protein signaling complexes; Phosphodiesterase 3B, Rap guanine nucleotide exchange factor 3, Therapeutic cancer target, Signaling pathway

Posted Date: August 10th, 2021

DOI: https://doi.org/10.21203/rs.3.rs-763041/v1

Abstract

Background

Protein signaling complexes play important roles in prevention of several cancer types and can be used for development of targeted therapy. The roles of signaling complexes of phosphodiesterase 3B (PDE3B) and Rap guanine nucleotide exchange factor 3 (RAPGEF3), which are two important enzymes of cyclic adenosine monophosphate (cAMP) metabolism, in cancer have not been fully explored.

Methods

The natural product Kaempferol-3-O-(3",4"-di-E-p-coumaroyl)-α-L-rhamnopyranoside designated as KOLR was extracted from *Cinnamomum pauciflorum* Nees leaves using reverse phase chromatography, high-resolution mass spectrometry, and nuclear magnetic resonance spectroscopy. The antitumor effect of KOLR was analyzed by multiple cell proliferation and metastasis experiments. The PDE3B/RAPGEF3 complex was found to be the target of KOLR through mRNA sequencing, Co-Immunoprecipitation assay, gene knock-down, gene mutation of drug-resistance cell line, and molecular docking. In vivo studies have shown that KOLR has the same antitumor mechanism.

Results

KOLR exhibited cytotoxic effects against selected cancer cells, except for AsPC-1 pancreatic cancer cell line. KOLR stabilized PDE3B/RAPGEF3 signaling complex thus inhibiting AKT phosphorylation and Rap-1 activation. Notably, mutation of RAPGEF3 G557A inhibited effect of KOLR on stabilizing PDE3B/RAPGEF3 complex in AsPC-1 cells. Furthermore, downregulation of PDE3B expression inhibited cytotoxic effect of KOLR on tumor cells. Downregulation of RAPGEF3 and Rap-1 expression promoted apoptosis of tumor cells and inhibited tumor metastasis. PDE3B inhibits activity of RAPGEF3 and activation of downstream signaling pathway.

Conclusion

The findings of this study show that KOLR could stabilize PDE3B/RAPGEF3 signaling complex to play an anti-tumor role and the PDE3B/RAPGEF3 complex is a potential therapeutic cancer target.

1. Background

Approximately 19.3 million new cancer cases and almost 10.0 million cancer deaths were reported in 2020 globally [1]. Although targeted and immunomodulatory drugs are effective in a subset of cancer patients [2,3], most cancer patients do not respond to these treatments towing to drug resistance and severe side effects. Therefore, studies should explore new targets and discover effective drugs for the

treatment of various cancers. Phenotypic screening for new anticancer agents against different cancer cell lines can be used to discover novel targets for cancer therapy and help in elucidating the specific molecular mechanism [4,5]. Protein-protein interactions (PPIs) and protein complexes play important roles in regulation and execution of most biological processes and are regarded as phenotypic screening targets in cells [6,7].

Cyclic adenosine monophosphate (cAMP) is a second messenger and plays important role in most biological functions, including cardiac contraction, energy homeostasis, cell metabolism, and ion channel activation [8-10]. Intracellular cAMP concentrations are regulated by coordinated activities of adenylyl cyclases (ACs) and cyclic nucleotide phosphodiesterases (PDEs). G protein-coupled receptors (GPCRs) signaling activates ACs leading to generation of cAMP in cells [11]. PDEs control cellular content of cyclic nucleotides and recruit them into multiprotein signaling complexes by forming individual pockets or nanodomains of cyclic nucleotide signaling [12-14].

Protein kinase A (PKA) and Rap guanine nucleotide exchange factor (RAPGEF, also known as exchange protein directly activated cAMP, EPAC) are intracellular cAMP effectors implicated in regulation of several physiological processes [15-17]. PKA and EPAC1 have a cyclic nucleotide-binding domain (CNBD) domain with similar affinities for cAMP binding [18] and can act synergistically, antagonistically, or independently [19]. Previous studies reported that RAPGEF proteins are involved in several biological processes, including proliferation and migration/metastasis of cancer cells [19], cardiomyocyte hypertrophy [20], insulin secretion [21], and depression [22]. RAPGEF activates Rap-1 signaling pathway, extracellular response kinase 1/2 (ERK1/2), and phosphoinositide 3-kinase (PI3K)/protein kinase B (Akt) signaling pathways, which are important signaling pathways involved in cancer progression. Most studies report a pro-proliferative and pro-metastatic role of RAPGEF in many cancers, whereas some contradictory effects of RAPGEF are reported in different tumors and cell types [19]. RAPGEF forms several molecular complexes with different proteins such as β-arrestin2, β-catenin, and PDEs to perform different biological functions [23-25].

In the current study, an anti-tumor natural product Kaempferol-3-O-(3",4"-di-E-p-coumaroyl)-α-L-rhamnopyranoside designated as KOLR was extracted from *Cinnamomum pauciflorum* Nees leaves. KOLR promoted apoptosis in selected cancer cells, whereas it did not show any effect on AsPC-1 pancreatic cancer cells. KOLR exerted its effect by stabilizing PDE3B/RAPGEF3 signaling complex. PDE3B inhibits activity of RAPGEF3 and activation of the downstream signaling pathway. The PDE3B/RAPGEF3 protein complex plays a key role in inhibiting cell growth and metastasis. The findings of the current study show that PDE3B/RAPGEF3 complex is potential therapeutic cancer target.

2. Methods

2.1 Isolation and purification of KOLR from leaves of *Cinnamomum pauciflorum Nees*

Cinnamomum pauciflorum Nees leaves were crushed into powder using high-speed multifunctional mill. 50 g of the powder was weighed and added to ethanol at a mass to volume ratio of 1:10. The powder

was soaked and extracted overnight in a shaker at room temperature, then centrifuged at 3000 rpm for 15 min. The supernatant was collected as ethanol extract (100 mg/mL). Different concentrations (30%, 50%, 70%, and 100%) of ethanol were used to separate the extracts through C18 trans separation solid-phase extraction cartridges InertSep (GL Sciences, Netherlands), and the washed components were collected. Analytical high performance liquid chromatograph (HPLC) was used for qualitative analysis of anti-tumor active components, and bioassays were performed to explore the anti-tumor activity. Active compounds were analyzed using high-performance liquid phase, C18 column, mobile phase comprising acetonitrile: water =55:45, and detection performed at a wavelength of 275 nm. The collected sample was concentrated to eliminate acetonitrile by pressure reduction and then freeze-dried to obtain a solid. Characterization of a single active ingredient was performed by vacuum drying at room temperature. The active compounds were identified by high-resolution mass spectrometry and nuclear magnetic resonance (NMR) spectroscopy.

2.2 Cancer cell lines culture

All cancer cells were purchased from Procell (Wuhan, China) and Cell Bank, Chinese Academy of Science (Shanghai, China). Cell lines were cultured in modified 1640 medium (Biological Industries) or Dulbecco Minimal Essential Medium (DMEM, Biological Industries) with 10% fetal bovine serum (FBS, Biological Industries) under a humidified incubator containing 5% CO_2 at 37°C. All cancer cells grew adherently. Cancer cells in the logarithmic growth phase were selected for further experiments.

2.3 Cancer cell proliferation assays

Cells were seeded into 96-well plates at a density of 5×10^3 cells/100 μL in 1640/ DMEM medium containing 10% FBS. After culturing overnight, different concentrations of extracts or growth factors such as KOLR, IGF, and VEGF were added in 3 replicates. Cells in each well were treated with 10 μL CCK8 (ApexBio), and the absorbance was measured at 450 nm at different time points. Cell survival rate was calculated by GraphPad Prism 8.

2.4 Cancer cell colony formation assay

Cells were digested with trypsin, and the BxPC-3 cells were plated in a 6-well plate at a density of 1×10^3 cells/2 mL. Cells were cultured overnight in an incubator for 24h. After cells adhered to the wall, KOLR at a final concentration of 2.5, 5, and 10 μg/mL was added and incubated for 15 days. Methanol was washed off using PBS and cells were stained with 0.4% crystal violet solution for 20 min. The crystal violet solution was washed off using PBS. Cells were observed and images collected under a microscope, and the number of BxPC-3 cells forming clones was determined.

2.5 Cancer cell EdU assay

Cells were digested with trypsin, and cultured into BxPC-3 cells in a 96-well plate with 1×10^4 cells/well. After cell adherent, cells were treated with KOLR at a concentration of 2.5, 5, and 10 μg/mL for 24 h, and

then 50 μL of the culture medium was extracted. 50 μL complete medium containing EdU (final concentration of 10 μm) it was added and incubated in an incubator for 2 h. Cells were washed once with PBS, fixed with 4% paraformaldehyde at room temperature for 15 min, washed three times with phosphate buffer (PBS), permeated with 0.5% TritonX-100 for 20 min, then wash three times with PBS. Click reaction solution (1× EDU reaction Buffer, CuSO4, Cy3 Azide, 1× EDU Buffer) was added for reaction under the dark condition at room temperature for 30 min. Samples were washed thrice with PBS, stained with 1×Hoechst 33342 under dark conditions at room temperature for 30 min then washed with PBS. Cells were observed and images collected under a fluorescence microscope, and the number of newly proliferated cells was determined.

2.6 Apoptosis of cancer cells

Trypsin digested cells were seeded in a system of 3×10^5 cells/well into a six-well plate. After culturing overnight, the medium was changed and different concentrations of KOLR were added and incubated for 24 h. Trypsin digestion was followed by centrifugation at 1000 RPM for 5 min to collect dead and living cells. Cells were resuspended with 400 μL 1×assay buffer (prepared with deionized water) and transferred to flow tubes. Cells were stained with 5 μL PI and FITC for 15 min at room temperature. Flow cytometry was used to observe cell apoptosis. FlowJO 7.6.1 software was used to analyze data and calculate the cell apoptosis rate.

2.7 Cancer cell cycle assay

BxPC-3 cells were seeded into a 6-well plate at 3×10^5 cells /well, and cultured overnight in an incubator for 24 h. The culture medium (containing 10% FBS) was changed and KOLR was added for 12 h. Trypsin digestion was performed followed by PBS washing. Cells were centrifuged at 300 g for 5 min to collect the living cells. Cells were fixed at 4℃ with 75% ethanol (prepared with deionized water) for 6 h and centrifuged at 700 g for 5 min to remove ethanol. Further, cells were washed twice with PBS, then 450 μL PI dye was added and transferred to a flow tube. Cells were stained at room temperature in dark for 15 min, and cell cycle was detected by flow cytometry.

2.8 Cancer cell invasion assay

Cancer cells were seeded in 6-well plate at 5×10^4 cells/well and placed into a chamber containing 50 μL matrix glue, and 650 μL complete medium containing 10% FBS was added to the lower chamber. KOLR was added and cells incubated for 48 h. The chambers were removed and fixed with methanol for 20 min. After staining with 0.1% crystal violet (PBS) for 20 min, cells in the chambers were wiped off with cotton swabs. Cells were observed and images collected under an inverted microscope. Number of cells passing through the chambers was determined.

2.9 Cancer cell wound-healing assay

Cancer cells in the logarithmic growth phase were seeded into a six-well plate at a density of 4×10^5/well and covered with wound healing experimental plug-ins. The plug-ins were placed in an incubator and cultured for 24 h. Plug-ins were removed, then the complete medium was replaced and KOLR was added. Images were obtained at 0 h and 24 h and area of the scratches was calculated with Image J.

2.10 RNAseq of BxPC-3 cells

BxPC-3 cells were seeded into a 6-well plate at a density of 3×10^5 cells/well, incubated for 12 h. 20 μg/mL YC was added for 12 h, cells were washed with PBS, and 800μL Trizol was added to each well to dissolve. Library preparation was performed following NEB common library construction method and sequencing was performed at Novogene company laboratories. HISAT2 was used to evaluate the quality of the original data and analyze the reference sequence. Correlation analysis between gene expression level and samples was performed by FPKM. Differential genes were screened by DEseq2. Clusterprofiler was used for KEGG pathway analysis of differential gene sets.

2.11 Western blot assay

Cancer cells were seeded in a 6-well plate at a density of 3×10^4 cells/well. After overnight incubation, cells were treated with different concentrations of KOLR for 24 h. Cell lysates were prepared by RIPA lysis and centrifuged at 12000 rpm/min for 15 min to separate the soluble components. Protein concentration was determined using a BCA protein detection kit following the manufacturer's instructions with slight modifications. A solution of 30 μg/mL was prepared with RIPA lysate, and the protein fragments were boiled in a metal sampler for 5 min. Samples containing 20-50 μg total protein were isolated on 8%-15% SDS-PAGE gel. The protein was transferred from the gel to nitrocellulose membrane (PALL) at a constant current at 300 mA for 90 min. Protein sample was sealed with 3% BSA for 1 h at room temperature and incubated overnight with the corresponding primary antibody (diluted by 3% BSA) in an antibody incubator box. Protein sample was washed three times with TBST. Goat anti-rat and anti-rabbit IgG were used as secondary antibodies and incubated at room temperature for 1 h, then washed three times with TBST. Chemiluminescence kit and chemiluminescence imager were used to detect the imprinting region. Image J was used to determine area of the imprinting region.

2.12 Indirect immunofluorescence

Cancer cells and KOLR treated cancer cells were seeded in a 48-well plate at a density of 1.5×10^4/well. Cell samples were treated with KOLR after cell adhesion for 24 h. Cells were washed three times with PBS, fixed with 4% paraformaldehyde for 15 min, and permeated with 0.5% TritonX-100 for 20 min. 3% BSA was added to samples and incubated for 1 h. Primary antibody was diluted at 1:5000 and incubated with cells in a shaker at room temperature for 1 h, then samples were washed with PBST. Diluted fluorescent secondary antibody was added to cells and incubated in a shaker at room temperature for 1 h, then washed by PBST. 100 μL DAPI was added to each well, stained for 15 min, add anti-fluorescence sealing tablets and nail oil sealing tablets were added. Cells were observed and images collected under a confocal microscope.

2.13 Co-Immunoprecipitation assay

After KOLR treatment, BxPC-3 cells were transferred to EP tubes at a density of 1×10^7/EP tube. After IP lysis/washing buffer was used for cell lysis for 30 min, then the cell precipitate was removed by centrifugation at 10000 g for 10 min. Protein concentration was determined using a modified BCA protein quantitative kit. Protein concentration in the cells was diluted to 1.5 mg/mL with IP lysis/scrubbing buffer. 500 µl protein lysate was added into a centrifuge tube containing antibody coupled magnetic beads and incubated overnight on a rotator at low temperature (magnetic beads were suspended during incubation). Magnetic beads were collected with the magnetic rack to remove unbound samples. 500 µL immunoprecipitation (IP) lysis/scrubbing buffer was added to the centrifuge tube, then samples were washed twice and gently mixed well. Magnetic beads were collected and the supernatant removed. 500µl ultra-pure water was added to the centrifuge tube and samples were washed once to remove the supernatant. 100 µL elution buffer was added to the centrifuge tube and incubated on a rotator at room temperature for 5 min. Magnetic beads were separated by a magnetic frame and the supernatant containing the target antigen was retained. Samples obtained by immunoprecipitation were used for determination of expression levels of the target antigen by western blot.

2.14 Immunohistochemistry

For Immunohistochemistry (IHC) analysis, deparaffinized DRG sections were boiled in sodium citrate buffer and incubated with primary antibodies p-Akt and Ki67 at 4 °C overnight. Immunostaining was performed using 3,3’-diaminobenzidine-tetrahydrochloride-dihydrate and samples were counterstained with hematoxylin. Negative controls were processed without the primary antibody. Nuclei were blue after hematoxylin staining and the positive expression of DAB was brownish-yellow.

2.15 Small interfering RNA (siRNA) knockdown RAPGEF3/RAP1A/PDE3B

Cancer cells were seeded into a six-well plate at a density of 3×10^5 cells /well. After incubation for 12 h, cells were washed twice with OPTIM-MEM (Gibco, Massachusetts, USA). Cells were then transfected with siRNA (final concentration 75 nM) for 48 h using Lipofectamine 2000 (Invitrogen, Carlsbad, CA), following the manufacturer’s instructions. siRNA sequences are shown in Table 4S.

2.16 RNA extraction and qRT-PCR

Total RNA was extracted using the Trizol method (Haoke, China), and cDNA was generated by reverse transcription kit (Thermo, USA). Gene expression analysis was performed by qRT-PCR using an SYBR Premix Kit (Apibixo). Relative gene expression was quantified using the comparative threshold cycle ($2^{-\Delta\Delta Ct}$) method. Sequences of the primers used in qRT-PCR (Qingke Biological Technology Services Co., Ltd, China) are shown in Table 5S

2.17 Molecular docking

Tertiary (3D) structure of RAPGEF3 was built through homology modeling using Modeller. Secondary and tertiary structures of PDE3B were modeled from scratch by RaptorX and Rosetta as the N-terminal tertiary structure of PDE3B was missing. RAPGEF3 and PDE3B protein-protein docking was performed using Rosetta software. Autodock was used for docking of KOLR ligands to proteins.

2.18 Xenograft mouse model

All animal studies were approved by the Animal Care Ethics Committee of Zhejiang Academy of Traditional Chinese Medicine. Male BALB/c nude mice (4 weeks old) were purchased from the Zhejiang Academy of Medical Science. BxPC-3 cells were injected subcutaneously on the left flanks of each mouse at a density of 1.5×10^6 cells/100μL. After the tumor size was approximately 100 mm^3, KOLR was administered at a dose of 25 and 50 mg/kg through intraperitoneal (i.p.) route for 5 days and tumor size was determined every day. Tumor size was determined using the equation V (in mm^3) = $0.52\times length\times width^2$. Nude mice were sacrificed by anesthesia cervical dislocation, and tumors were harvested for further analysis.

2.19 Statistical analysis

For all *in vivo* and *in vitro* experiments, a two-tailed students test was performed using GraphPad 8.0. All experimental data were reported as mean ± SD or mean ± SEM. Differences were considered statistically significant at P<0.05, and the statistical significance was shown as*$p < 0.05$**$p < 0.01$; and ***$p < 0.001$.

3. Results

3.1 KOLR inhibits cancer cell proliferation and tumor growth

Crude extracts of *Cinnamomum pauciflorum* Nees showed anti-tumor effects against several cancer cell lines, with significant effects observed for pancreatic cancer BxPC-3 cell line (Figure 1 and S1A). Antitumor effect of 50% ethanol extract obtained through the C18 separation column showed significant effects (Figure S1B). KOLR compound was the main active ingredient identified using high-resolution mass spectrometry and nuclear magnetic resonance (NMR) by comparing to a reference compound (Figure S1 and S2, Table 1S and 2S). KOLR showed significant inhibition activity against proliferation and colony formation of BxPC-3 cell line in a dose- and time-dependent manner (Figure 1). Notably, KOLR showed different activities against different cell lines, with an IC50 14.4 μg/mL (19.9 μM) for BxPC-3 cells (Table 3S). Structure of KOLR including Kaempferol, α-L-rhamnopyranoside, and p-hydroxy-cinnamic acid was elucidated (Figure 1 and S3). The IC50 of Kaempferol against BxPC-3 cells was approximately 100 μM, whereas trans-cinnamic acid, and p-hydroxy-cinnamic acid showed no significant anti-tumor effect (IC50>100 μM) (Figure S3A-D). These findings show that the different KOLR compounds apart from kaempferol had significant inhibitory effects against cancer cell proliferation *in vivo*. KOLR inhibited the effect of several pro-cancer factors such as arachidonic acid (AA), insulin-like growth factor (IGF-1), Platelet-activating factor (PAF), and vascular endothelial growth factor (VEGF) (Figure S3E-H).

To explore the mechanism of KOLR inhibition activity against cell proliferation, cell cycle and apoptosis of BxCP-3 cells treated with KOLR were explored. KOLR significantly promoted apoptosis of BxPC-3 cells in a dose-dependent manner and modulated cell cycle of BxPC-3 cells (Figure 2A and Figure S4A). KOLR modulated expression of apoptosis-related genes such as PARP1, Caspase 3, Caspase 9, and CDK4 in a dose-dependent manner (Figure 2A and Figure S4B). In addition, KOLR inhibited BxCP-3 cell invasion and wound healing ability (Figure 2B-E). Moreover, KOLR modulated expression of metastasis-related genes such as E-cadherin and β-catenin (Figure S4C). These findings indicate that KOLR promotes cancer cell apoptosis and inhibits tumor metastasis.

3.2 KOLR inhibits Rap-1 and PI3K-Akt signaling pathway

To explore the underlying antitumor molecular mechanisms of KOLR transcriptome sequencing of KOLR-treated BxPC-3 cells was performed by Novogene company (Figure S5A and B). KEGG pathway analysis showed that Rap-1 and PI3K-Akt signaling pathways were significantly down-regulated in KOLR-treated BxPC-3 cells (Figure 3A-B and Figure S5C). Indirect immunofluorescence analysis showed that KOLR significantly inhibited phosphorylation of Akt in BxPC-3 cells (Figure 3C). Expression of related genes of Rap-1 and PI3K-Akt signaling pathway were down-regulated, mainly phosphorylated Akt (p-Akt), phosphorylated ERK, phosphorylated mTOR (p-mTOR), PI3K p85, and PI3K γ110 (Figure 3D-F). Furthermore, KOLR inhibited activation of Rap-1 in BxPC-3 cells as shown by analysis using Rap-1 activity detection reagent kit (Figure 4A). To further explore the role of the Rap-1 signaling pathway in tumors, siRNA-RAP1A was used to perform Rap1 knockdown. Downregulation of RAP1A expression downregulated expression of EPAC1, p-Akt and p-ERK (Figure 4B and C). Further, down-regulation of RAP1A expression promoted apoptosis of BxCP-3 cells and inhibited invasion of BxCP-3 cells (Figure 4E-F and Figure 6SA). These findings showed that KOLR inhibits Rap-1 and PI3K-Akt signaling pathways thus promoting cancer cell apoptosis and inhibiting tumor metastasis.

3.3 KOLR targets RAPGEF3/PDE3B complex

RAPGEFs mainly act as guanine nucleotide exchange factors that activate the small G proteins, Rap1. Apoptosis of BxCP-3 cells increased and invasion of BxCP-3 cells was inhibited after RNA interference with RAPGEF3 (Figure 4E-F and Figure 6SB). Rap-1, PI3K-Akt, and EKR1/2 signaling pathways were down-regulated by low expression levels of RAPGEF3 (Figure 4C). To further explore the target of KOLR, immunoprecipitation analysis was performed on KOLR treated BxCP-3 cells using RAPGEF3 antibody. The findings showed a decrease in protein concentration of RAPGEF3, PI3K γ110, Akt, and RAP1A/B, however, concentration of PDE3B increased in BxCP-3 cells with an increase in KOLR concentration (Figure 5A). Laser confocal analysis showed that KOLR induces aggregation of PDE3B and RAPGEF3 resulting in co-localization in the cytoplasm (Figure 5B). These findings indicated that KOLR promoted binding between RAPGEF3 and PDE3B, and inhibited binding between PI3Kγ110 and Akt. To further explore the function of PDE3B in the RAPGEF3/PDE3B complex, RNA interference of PDE3B was performed. The findings showed no change in apoptosis and invasion of BxPC-3 cells after PDE3B RNA interference compared with the control (Figure S7). Downregulation of PDE3B increases the resistance of

BxCP-3 to KOLR (Figure 5C-F). Molecular docking experiments showed that a stable complex was formed between KOLR and RAPGEF3/PDE3B (Figure S8 and Table 4S). Notably, two different binding modes were observed depending on the order of binding (Figure S8 and Table 4S). These findings showed KOLR targets to RAPGEF3/PDE3B complex to inhibit Rap-1 and PI3K-Akt signaling pathways.

3.4 Mutation of RAPGEF3 G557A affects targeting of KOLR

The findings of the current study showed that AsPC-1 cells were resistant to KOLR (Table 3S), whereas expression of RAPGEF3 and RAP1A affected invasion of AsPC-1 cells but not apoptosis of these cells (Figure S8). Protein levels of RAPGEF3, Akt, and RAP1A/B did not show differences after treatment with KOLR. Notably, PI3Kγ110 expression level was weakly decreased, however, PDE3B protein level in AsPC-1 cells was slightly increased by treatment with KOLR but not in a dose-dependent manner (Figure 5G). Further analysis showed a mutation of RAPGEF3 G557A in AsPC-1 (Figure 6A). Furthermore, the three-dimensional structure RAPGEF3 WT and RAPGEF3 G557A were built and molecular dynamics of RAPGEF3 WT and RAPGEF3 G557A were performed. After the mutation to A557, the hydrophobic -CH_3 of the alanine side chain formed an interaction and steric hindrance with the polar hydrophilic -C=O-NH_2 of the side chain of the adjacent amino acid N552 (Figure 6B). The average structure of RAPGEF3 (G557) was significantly different from the structure of the mutant RAPGEF3 (A557), mainly in the vicinity of residue 557 (Figure 6C). This change in structure resulted in a significant phase shift of the overall structure. Moreover, size of the binding pocket of PDE3B and KOLR was significantly decreased in the wild-type protein (Figure 6C). The global energy for molecular docking was significantly different between KOLR and wild-type and mutant RAPGEF3 (Figure 10S). Structure of RAPGEF/PDE3B/KOLR complex was changed by G557A mutation (Figure 6D). The -OH groups on KOLR formed polar hydrogen bonds with surrounding amino acids (S478, A527, R514, P529, Q555, and D558,) whereas the benzene ring of KOLR formed hydrophobic interactions with the surrounding hydrophobic amino acids (A553, C552, L520, P529, A527, C517, L480, and V473) in the wild-type RAPGEF3 (Figure 10SC). In addition, the -OH on KOLR formed polar hydrogen bonds with surrounding amino acids (Q151, F237, R798, R801, D821, and A848), and the benzene ring of KOLR formed hydrophobic interactions with the surrounding hydrophobic amino acids (L804, K820, M822, M851) with the mutant RAPGEF3 G557A (Figure 10SD). These findings showed that KOLR binding to RAPGEF3/PDE3B complex and RAPGEF3 G557A mutant leads to KOLR resistance.

3.5 KOLR inhibits growth of transplanted tumor *in vivo*

To further explore the anti-tumor effect of KOLR *in vivo*, the anti-tumor effects of KOLR were determined using a mouse tumor growth model xenotransplant. Nude mice were subcutaneously administered with BxPC-3 cells to achieve approximately 100mm^3 tumor size. Mice were then randomly divided into three groups including: control, 25mg/kg, and 50mg/kg. KOLR was administered intraperitoneally for five consecutive days and tumor sizes were recorded each day. Mice were sacrificed on the sixth day and analysis showed that KOLR exhibits anti-tumor efficacy at a concentration of 50mg/kg (Figure 7A and B). Western blot analysis showed that antitumor mechanism of KOLR *in vitro* was consistent with *in vivo* mechanisms (Figure 7C). Consistently, immunohistochemistry (IHC) assay showed that expression levels

of p-Akt and the proliferation marker Ki67 were all significantly decreased *in vivo* after administration with 50mg/kg KOLR, compared with levels in the control group (Figure 7D). In summary, these findings show that KOLR targets RAPGEF3/PDE3B complex and promotes binding of the complex to exhibit antitumor effects *in vitro* and *in vivo* (Figure 7E).

4. Discussion

It is important to find new targets or biomarkers for cancer therapy owing to limited efficacy of conventional therapy approaches. The findings of the current study showed that the natural product KOLR extracted from *Cinnamomum pauciflorum* Nees leaves targets RAPGEF3/PDE3B complex to exert cytotoxic effects on cancer cells.

KOLR comprised kaempferol, rhamnopyranoside, and two p-hydroxy-cinnamic acids. These compounds are found in several medicinal plants such as *Laurus nobilis* and *Epimedium sagittatum* [26,27]. Kaempferol and p-hydroxy-cinnamic acid have anti-inflammatory, anti-oxidant, and anti-tumor activities [28-30]. Notably, the findings showed that the antitumor effect of KOLR against BxPC-3 cell line was significantly higher compared with that of kaempferol and p-hydroxycinnamic acid. The findings showed that KOLR has a novel antitumor target in the BxPC-3 cell line. Binding to this target inhibited growth of tumor cells induced by several cell growth factors.

cAMP is an important intracellular second messenger that plays an important role in tumor growth and progression. Previous studies report that RAPGEF is an important anticancer target owing to its role in downstream pathways such as Rap-1, PI3K/Akt, EKR1/2, and β-catenin implicated in carcinogenesis and cancer progression [19]. Rap-1 and PI3K-Akt signaling pathways were significantly downregulated in BxPC-3 cells after KOLR treatment (Figure 3). The findings indicated that RAPGEF3 is a potential therapeutic target for KOLR. The RAPGEF specific inhibitor ESI-09 inhibits cell proliferation and migration in different cell lines [31-33]. The findings of the current study showed that apoptosis was promoted and metastasis was inhibited in BxCP-3 cells knockout of RAPGEF3, however, knockout of RAPGEF3 in AsPC-1 cells only inhibited metastasis but did not affect apoptosis. In addition, AsPC-1 cells showed higher resistance rate to ESI-09 and KOLR compared with BxPC-3 cells. The findings showed a difference in the role of RAPGEF3 in AsPC-1 compared with BxPC-3 cells. Further, RAPGEF3 G557A mutant was identified in AsPC-1 cells, and the mutation affected binding of the PDE3B/RAPGEF3 complex. The role of this mutation in promoting the function of AsPC-1 cells should be further explored.

Protein-protein interactions (PPIs) and protein complexes are important in regulation and execution of most biological processes. A study on cell adhesion reported a signaling complex containing PDE3 activity and RAPGEF3 in HEK 293T cells, and immunoblot analysis showed that PDE3 activity was attributed to the presence of PDE3B [25]. The N terminal fragment of PDE3B binds to RAPGEF3, and heterologous overexpression of the N terminal fragment of PDE3B antagonizes PDE3B/RAPGEF3 complex formation in cells [25,34]. In addition, PDE3B/RAPGEF3 signalosome modulates functions of human arterial endothelial cells (HAECs) implicated in angiogenesis by integrating cAMP- and PI3Kγ-

encoded signals [34]. Current family-specific PDE3 inhibitors such as cilostamide and milrinone inhibit activity of PDE3, irrespective of their intracellular signaling network and enzyme inhibition alone is not sufficient for cell death [35]. The findings of the current study showed that KOLR promoted formation of the RAPGEF3/PDE3B complex thus inhibiting activation of PI3K/Akt and Rap-1 signal pathway and cell proliferation. High expression level of PDE3B is correlated with a better prognosis in a variety of tumors such as lung cancer, colon cancer and pancreatic cancer (https://www.proteinatlas.org/ENSG00000152270-PDE3B/pathology). These activities can be attributed to RAPGEF3-PDE3B interactions that decrease concentration of cAMP around RAPGEF3 in cells, by occupying the binding site of Rap-1, and failure of allosteric activation of RAPGEF3.

Although PPI modulators are currently dominated by inhibitors, some PPI-stabilizing natural products have been used as important drugs such as Paclitaxel, which stabilizes polymerized microtubule structures [36]. DNMDP induces complex formation between phosphodiesterase 3A (PDE3A) and schlafen family member 12 (SLFN12) to kill cancer cells, whereas PDE3B promotes DNMDP sensitivity in the absence of PDE3A [35,37,38]. Similar to these PPI small-molecule stabilizers, KOLR stabilizes and induces RAPGEF3/PDE3B complex formation to inhibit Rap-1 and PI3K/Akt signaling pathways in different cell lines. Further studies are required to explore more active compounds that promote RAPGEF3/PDE3B formation and to elucidate the functional differences of RAPGEF3/ PDE3B complex in different cells.

5. Conclusion

In summary, this research showed that KOLR stabilizes and induces RAPGEF3/PDE3B complex formation to inhibit Rap-1 and PI3K/Akt signaling pathways. This study has uncovered a previously unknown role of the RAPGEF3/PDE3B complex in killing cancer cells and the findings show that RAPGEF3/PDE3B complex can be used as a new therapeutic target against cancer.

Abbreviations

phosphodiesterase 3B: PDE3B; Rap guanine nucleotide exchange factor 3: RAPGEF3; cyclic adenosine monophosphate: cAMP; Kaempferol-3-O-(3",4"-di-E-p-coumaroyl)-α-L-rhamnopyranoside: KOLR; Protein-protein interactions: PPIs; adenylyl cyclases: ACs; phosphodiesterases: PDEs; G protein-coupled receptors: GPCRs; Protein kinase A: PKA; exchange protein directly activated cAMP: EPAC; cyclic nucleotide-binding domain: CNBD; extracellular response kinase 1/2: ERK1/2; phosphoinositide 3-kinase: PI3K; protein kinase B: Akt; high performance liquid chromatograph: HPLC; nuclear magnetic resonance: NMR; Dulbecco Minimal Essential Medium: DMEM; fetal bovine serum: FBS; phosphate buffer: PBS; immunoprecipitation: IP; Immunohistochemistry: IHC; arachidonic acid: AA; insulin-like growth factor: IGF-1; Platelet-activating factor: PAF; vascular endothelial growth factor: VEGF; human arterial endothelial cells: HAECs; phosphodiesterase 3A: PDE3A; schlafen family member 12: SLFN12

Declarations

Ethics approval and consent to participate

All animal experiments were approved by the Animal Ethics Committee of Zhejiang Academy of Traditional Chinese Medicine and conducted according to the Guidelines for the Care and Use of Animals for Scientific Research.

Consent for publication

All authors have read and agreed to publish this manuscript.

Competing interests

The authors declare no conflict of interest.

Funding

This work was supported by the National Natural Science Foundation of China (Grant No: 82074093, 81673809, 81673781), Natural Science Foundation of Zhejiang Province (Grant No: LY19H280005), The Scientific and Technological Program of Sichuan province (Grant No: 20YYJC4341), and Zhejiang Traditional Chinese Medicine Administration (Grant No: 2020ZX003, 2021AX002, and 2016ZQ002).

Acknowledgments

Not applicable

Author contributions

MQL, QL, and KQC designed this research. MQL, FL, GPC, JBC, JLC, JCL, LYD, ZH Y, YF W, JL, YYL, YQZ participated in various experimental parts of the implementation of the project and discussed the results. MQL, FL, QL, and KQC wrote the manuscript and made the figures. MQL, FL contributed equally to this work. All authors read and approved the final manuscript.

Author details

1. Cancer Institute of Integrated tradition Chinese and Western Medicine, Zhejiang Academy of Traditional Chinese Medicine, Tongde Hospital of Zhejiang Province, Hangzhou, Zhejiang, 310012, China

2. Zhejiang Provincial Key Laboratory of Cancer Prevention and Treatment Technology of Integrated Traditional Chinese and Western Medicine, Hangzhou, Zhejiang, 310012, China

3. College of Life Science, Sichuan Normal University, Chengdu, Sichuan, 610101, China

4. People's Liberation Army Joint Logistic Support Force 903th Hospital, Hangzhou, Zhejiang, 330000, China

References

1. Sung H, Ferlay J, Siegel RL, Laversanne M, Soerjomataram I, Jemal A, Bray F. Global cancer statistics 2020: GLOBOCAN estimates of incidence and mortality worldwide for 36 cancers in 185 countries. CA Cancer J Clin. 2021. doi:10.3322/caac.21660.
2. Wang YX, Zhang S, Li FC, Zhou Y, Zhang Y, Wang ZW, Zhang RY, Zhu J, Ren YX, Tan Y, Qin C, Li YH, Li XX, Chen YZ, Zhu F. Therapeutic target database 2020: enriched resource for facilitating research and early development of targeted therapeutics. Nucleic Acids Res. 2020;48(D1):D1031–41. doi:10.1093/nar/gkz981.
3. Riley RS, June CH, Langer R, Mitchell MJ. Delivery technologies for cancer immunotherapy. Nat Rev Drug Discov. 2019 Mar;18(3):175–96. doi:10.1038/s41573-018-0006-z.
4. Swinney DC, Anthony J. How were new medicines discovered? Nat Rev Drug Discov. 2011;10(7):507–19. doi:10.1038/nrd3480.
5. Basu A, Bodycombe NE, Cheah JH, Price EV, Liu K, Schaefer GI, Ebright RY, Stewart ML, Ito D, Wang S, Bracha AL, Liefeld T, Wawer M, Gilbert JC, Wilson AJ, Stransky N, Kryukov GV, Dancik V, Barretina J, Garraway LA, Hon CSY, Munoz B, Bittker JA, Stockwell BR, Khabele D, Stern AM, Clemons PA, Shamji AF, Schreiber SL. An interactive resource to identify cancer genetic and lineage dependencies targeted by small molecules. Cell. 2013;154(5):1151–61. doi:10.1016/j.cell.2013.08.003.
6. Lin CY, Lee CH, Chuang YH, Lee JY, Chiu YY, Lee YHW, Jong YJ, Hwang JK, Huang SH, Chen LC, Wu CH, Tu SH, Ho YS, Yang JM. Membrane protein-regulated networks across human cancers. Nat Commun. 2019;10(1):3131. doi:10.1038/s41467-019-10920-8.
7. Ryan CJ, Kennedy S, Bajrami I, Matallanas D, Lord CJ.A Compendium of Co-regulated Protein Complexes in Breast Cancer Reveals Collateral Loss Events Cell Syst. 2017, 5(4):399–409.e5. doi: 10.1016/j.cels.2017.09.011.
8. Yan K, Gao LN, Cui YL, Zhang Y, Zhou X. The cyclic AMP signaling pathway: exploring targets for successful drug discovery (Review). Mol Med Rep. 2016;13(5):3715–23.
9. Almahariq M, Mei FC, Cheng XD. Cyclic AMP sensor EPAC proteins and energy homeostasis. Trends Endocrinol Metab. 2014;25(2):60–71. doi:10.1016/j.tem.2013.10.004.
10. Chin KV, Yang WL, Ravatn R, Kita T, Reitman E, Vettori D, Cvijic ME, Shin M, Iacono L. Reinventing the wheel of cyclic AMP: novel mechanisms of cAMP signaling. Ann N Y Acad Sci. 2002;968:49–64. doi:10.1111/j.1749-6632.2002.tb04326.x.
11. Dorsam RT, Gutkind JS. G-protein-coupled receptors and cancer. Nat Rev Cancer. 2007;7:79–94. doi:10.1038/nrc2069.
12. Baillie GS, Tejeda GS, Kelly MP. Therapeutic targeting of 3',5'-cyclic nucleotide phosphodiesterases: inhibition and beyond. Nat Rev Drug Discov. 2019;18(10):770–96. doi:10.1038/s41573-019-0033-4.
13. Ahmad F, Degerman E, Manganiello VC. Cyclic nucleotide phosphodiesterase 3 signaling complexes. Horm Metab Res. 2012;44(10):776–85. doi:10.1055/s-0032-1312646.

14. Al-Nema MY, Gaurav A. Protein-Protein Interactions of Phosphodiesterases. Curr Top Med Chem. 2019;19(7):555–64. doi:10.2174/1568026619666190401113803.
15. García-Morales V, Luaces-Regueira M, Campos-Toimil M. The cAMP effectors PKA and Epac activate endothelial NO synthase through PI3K/Akt pathway in human endothelial cells. Biochem Pharmacol. 2017;145:94–101. doi: 10.1016/j.bcp.2017.09.004. Epub 2017 Sep 11.
16. Namkoong S, Kim CK, Cho YL, Kim JH, Lee H, Ha KS, Choe J, Kim PH, Won MH, Kwon YG, Shim EB, Kim YM. Forskolin increases angiogenesis through the coordinated cross-talk of PKA-dependent VEGF expression and Epac-mediated PI3K/Akt/eNOS signaling. Cell Signal. 2009;21(6):906–15. doi:10.1016/j.cellsig.2009.01.038.
17. Cheng X, Ji Z, Tsalkova T, Mei F. Epac and PKA: a tale of two intracellular cAMP receptors. Acta Biochim Biophys Sin (Shanghai). 2008;40(7):651–62. doi:10.1111/j.1745-7270.2008.00438.x.
18. Dao KK, Teigen K, Kopperud R, Hodneland E, Schwede F, Christensen AE, Martinez A, Døskeland SO. Epac1 and cAMP-dependent protein kinase holoenzyme have similar cAMP affinity, but their cAMP domains have distinct structural features and cyclic nucleotide recognition. J Biol Chem. 2006;281(30):21500–11. doi:10.1074/jbc.M603116200.
19. Wehbe N, Slika H, Mesmar J, Nasser SA, Pintus G, Baydoun S, Badran A, Kobeissy F, Eid AH. Elias Baydoun. The Role of Epac in Cancer Progression. Int J Mol Sci. 2020;21(18):6489. doi:10.3390/ijms21186489.
20. Laudette M, Coluccia A, Sainte-Marie Y, Solari A, Fazal L, Sicard P, Silvestri R, Mialet-Perez J, Pons S, Ghaleh B, Blondeau JP. Lezoualc'h F. Identification of a pharmacological inhibitor of Epac1 that protects the heart against acute and chronic models of cardiac stress. Cardiovasc Res. 2019;115(12):1766–77. doi:10.1093/cvr/cvz076.
21. Henquin JC, Nenquin M. Activators of PKA and Epac Distinctly Influence Insulin Secretion and Cytosolic Ca^{2+} in Female Mouse Islets Stimulated by Glucose and Tolbutamide. Endocrinology. 2014 Sep;155(9):3274–87. doi:10.1210/en.2014-1247.
22. Zhou L, Ma SL, Yeung PKK, Wong YH, Tsim KWK, So KF, Lam LCW, Chung SK. Anxiety and depression with neurogenesis defects in exchange protein directly activated by cAMP 2-deficient mice are ameliorated by a selective serotonin reuptake inhibitor, Prozac. Transl Psychiatry. 2016;6(9):e881. doi:10.1038/tp.2016.129.
23. Berthouze-Duquesnes M, Lucas A, Saulière A, Sin YY, Laurent A-C, Galés C, Baillie G, Lezoualc'h F. Specific interactions between Epac1, -arrestin2 and PDE4D5 regulate adrenergic receptor subtype differential effects on cardiac hypertro-phic signaling. Cell Signal. 2013;25:970–80.
24. Jansen SR, Poppinga WJ, de Jager W, Lezoualc'h F, Cheng X, Wieland T, Yarwood SJ, Gosens R, Schmidt M. Epac1 links prostaglandin E2 to β-catenin-dependent transcription during epithelial-to-mesenchymal transition. Oncotarget. 2016;7:46354.
25. Raymond DR, Wilson LS, Carter RL, Maurice DH. Numerous distinct PKA-, or EPAC-based, signalling complexes allow selective phosphodiesterase 3 and phosphodiesterase 4 coordination of cell adhesion. CellSignal. 2007;19:2507–18.

26. Wang GJ, Tsai TH, Lin LC. Prenylflavonol, acylated flavonol glycosides and related compounds from Epimedium sagittatum. Phytochemistry. 2007, 682455–2464.
27. Fiorini C, David B, Fourasté I, Vercauteren J. Acylated kaempferol glycosides from Laurus nobilis leaves. Phytochemistry. 1998;47(5):821–4.
28. Imran M, Salehi B, Sharifi-Rad J, Gondal TA, Saeed F, Imran A, Shahbaz M, Fokou PVT, Arshad MU, Khan H, Guerreiro SG, Martins N. Estevinho LM. Kaempferol: A Key Emphasis to Its Anticancer Potential. Molecules. 2019;24(12):2277. doi:10.3390/molecules24122277.
29. Masayoshi Yamaguchi 1. Tomiyasu Murata 2, Mamoru Shoji 1, M Neale Weitzmann.The flavonoid p-hydroxycinnamic acid mediates anticancer effects on MDA-MB-231 human breast cancer cells in vitro: Implications for suppression of bone metastases. Int J Oncol. 2015;47(4):1563–71. doi:10.3892/ijo.2015.3106.
30. Sova M, Saso L. Natural Sources. Pharmacokinetics, Biological Activities and Health Benefits of Hydroxycinnamic Acids and Their Metabolites. Nutrients. 2020;12(8):2190. doi:10.3390/nu12082190.
31. Kumar N, Gupta S, Dabral S, Singh S, Sehrawat S. Role of exchange protein directly activated by cAMP (EPAC1) in breast cancer cell migration and apoptosis. Mol Cell Biochem. 2017 Jun;430(1–2):115–125. doi: 10.1007/s11010-017-2959-3.
32. Almahariq M, Tsalkova T, Mei FC, Chen H, Zhou J, Sastry SK, Schwede F, Cheng X. A novel EPAC-specific inhibitor suppresses pancreatic cancer cell migration and invasion. Mol Pharmacol. 2013 Jan;83(1):122–8. doi:10.1124/mol.112.080689.
33. Lv WC, Liu SX, Zhang Q, Yi Z, Bao XY, Feng YP, Ren YP. Downregulation of Epac Reduces Fibrosis and Induces Apoptosis Through Akt Signaling in Human Keloid Fibroblasts. J Surg Res. 2021;257:306–16. doi:10.1016/j.jss.2019.12.026.
34. Wilson LS, Baillie GS, Pritchard LM, Umana B, Terrin A, Zaccolo M, Houslay MD, Maurice DH. A Phosphodiesterase 3B-based Signaling Complex Integrates Exchange Protein Activated by cAMP 1 and Phosphatidylinositol 3-Kinase Signals in Human Arterial Endothelial Cells. J Biol Chem. 2011 May 6; 286(18): 16285–16296. doi: 10.1074/jbc.M110.217026.
35. Waal L, Lewis TA, Rees MG, Tsherniak A, Wu XY, Choi PS, Gechijian L, Hartigan C, Faloon PW, Hickey MJ, Tolliday N, Carr SA, Clemons PA, Munoz B, Wagner BK, Shamji AF, Koehler AN, Schenone M, Burgin AB, Schreiber SL, Greulich H, Meyerson M. Identification of cancer-cytotoxic modulators of PDE3A by predictive chemogenomics. Nat Chem Biol. 2016 Feb;12(2):102–8. doi:10.1038/nchembio.1984.
36. Xiao H, Verdier-Pinard P, Fernandez-Fuentes N, Burd B, Angeletti R, Fiser A, Horwitz SB, Orr GA. Insights into the mechanism of microtubule stabilization by Taxol. Proc Natl Acad Sci U S A. 2006;103(27):10166–73. doi:10.1073/pnas.0603704103.
37. Wu X, Schnitzler GR, Gao GF, Diamond B, Baker AR, Kaplan B, Williamson K, Westlake L, Lorrey S, Lewis TA, Garvie CW, Lange M, Hayat S, Seidel H, Doench J, Cherniack AD, Kopitz C, Meyerson M. Greulich H.Mechanistic insights into cancer cell killing through interaction of phosphodiesterase 3A

and schlafen family member 12. J Biol Chem. 2020 Mar 13;295(11):3431–3446. doi: 10.1074/jbc.RA119.011191.

38. Li DR, Chen J, Ai YW, Gu XQ, Li L, Che D, Jiang ZD, Li L, Chen S, Huang HW, Wang JW, Cai T, Cao Y, Qi XB, Wang XD. Estrogen-Related Hormones Induce Apoptosis by Stabilizing Schlafen-12 Protein Turnover. Mol Cell. 2019;75(6):1103–16. doi:10.1016/j.molcel.2019.06.040.

Figures

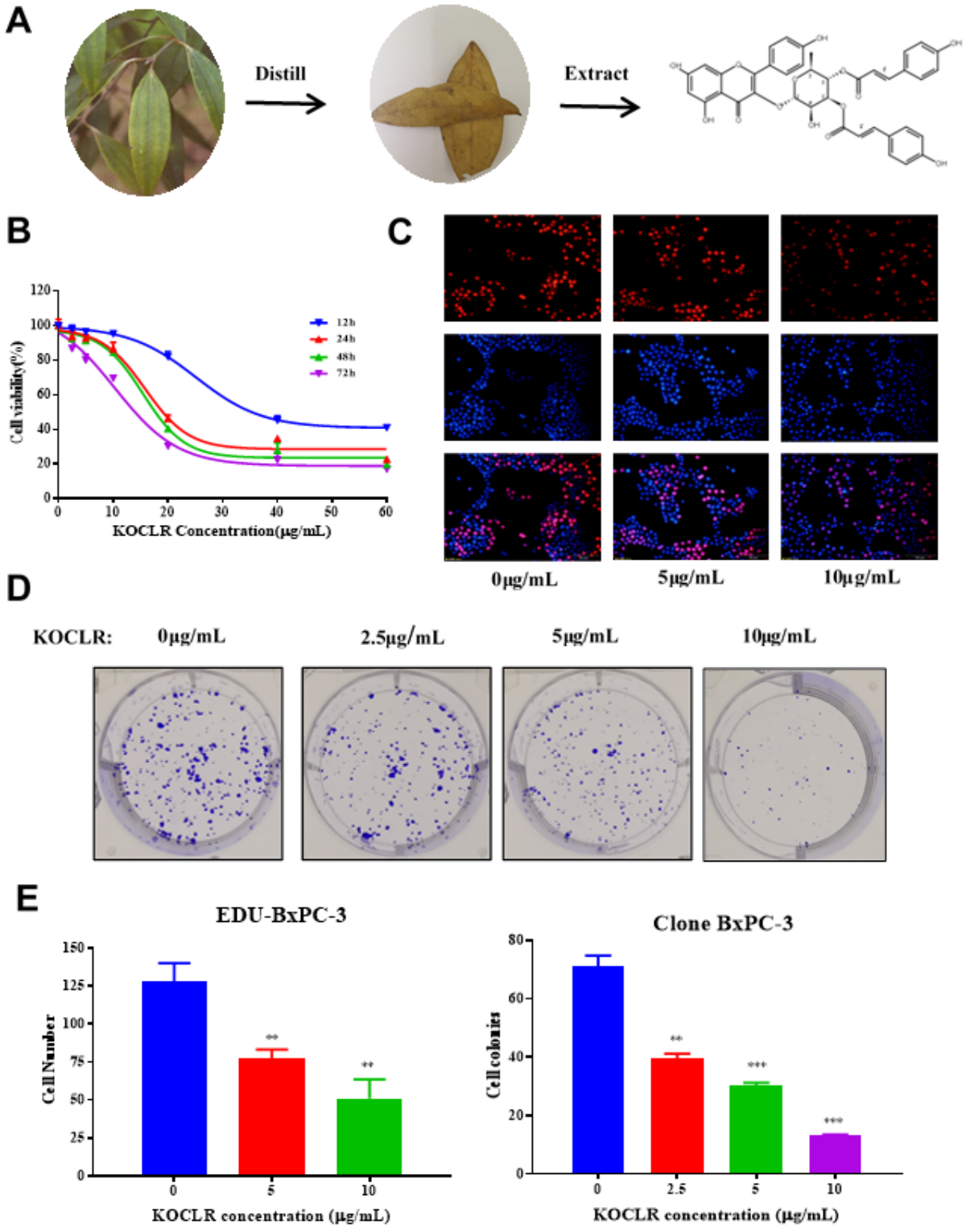

Figure 1

Effect of KOLR on proliferation of pancreatic cancer BxPC-3 cells. A. KOLR was extracted and purified from dried leaves of Cinnamomum pauciflorum Nees. B. Cell viability of pancreatic cancer BxPC-3 cells treated with different concentrations of KOLR at 12, 24, 48, and 72 h. C. BxPC-3 cell proliferation rate was determined using the EDU assay. D. BxPC-3 cells were exposed to various concentrations of KOLR for 15 days in colony formation assay. E. Number of EDU positive cells treated with different concentrations of

KOLR (n=3). F. Number of cell colonies treated with different concentrations of KOLR for 15 days (n=3). Data are expressed as mean ± SD or SEM of three independent experiments. Two-tailed students t-test was used, *p<0.05; **p<0.01; ***p<0.001.

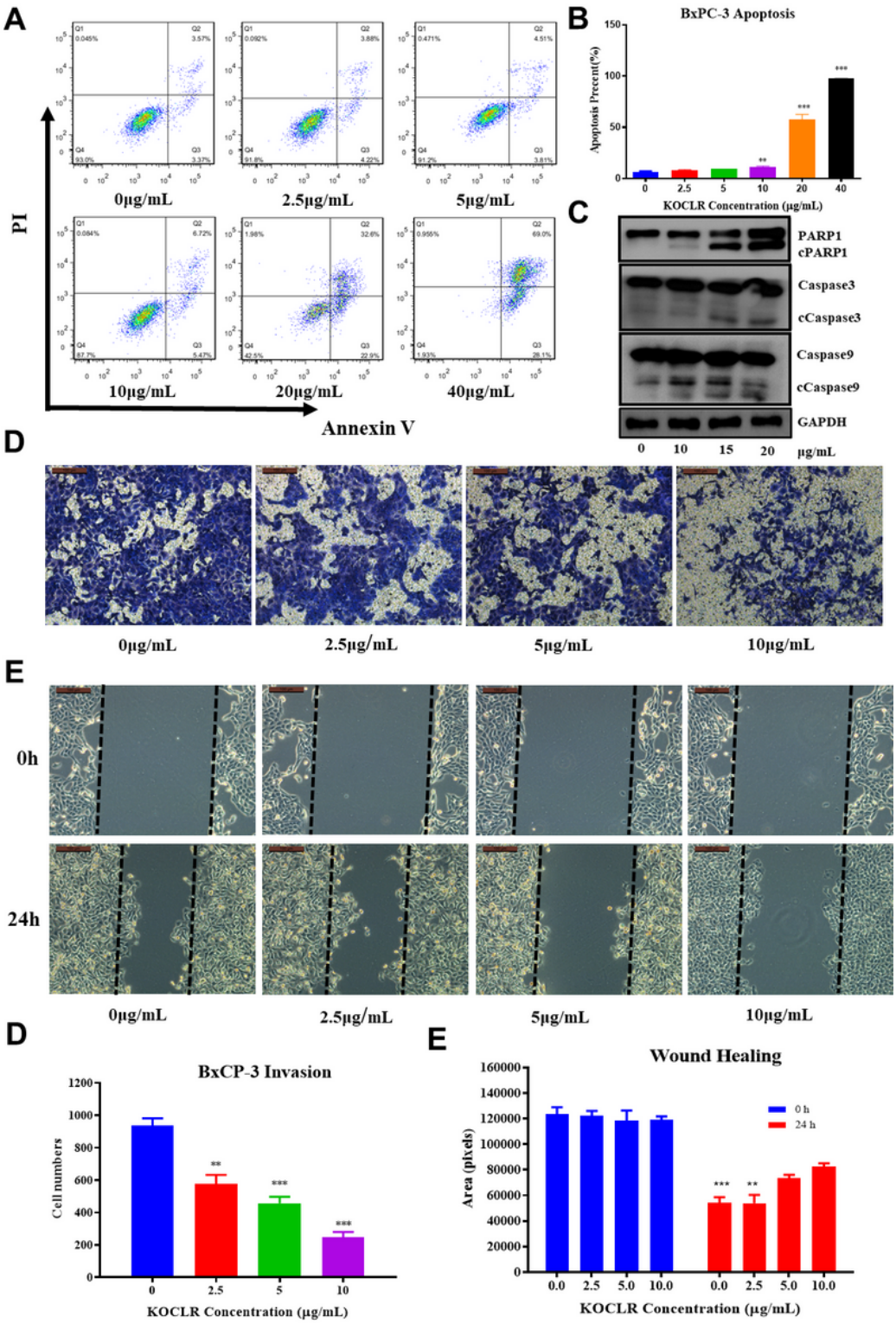

Figure 2

KOLR promotes apoptosis of BxCP-3 cells and inhibits BxCP-3 cell migration. A. Effects of KOLR on apoptosis of BxCP-3 cells by AnnexinV and propidium iodide double staining. B. Percentage of apoptosis

of BxCP-3 cells treated with different concentrations of KOLR (n=3). C. Protein expression levels of PARP1, Caspase9, and Caspase3 was determined by western blotting assays after treatment with different concentrations of KOLR. D. Invasion ability of BxCP-3 cells with different concentrations of KOLR was determined by transwell migration assay. E. Wound healing ability of BxCP-3 cells with different concentrations of KOLR was determined by scratch assay. F. Number of migratory BxCP-3 cells treated with different concentrations of KOLR is shown in the bar graphs (n=3). G. Wound healing area of BxCP-3 cells treated with different concentrations of KOLR is shown in the bar graphs (n=3). Data are expressed as mean ± SD or SEM of three independent experiments. Two-tailed students t-test was used, *p<0.05; **p<0.01; ***p<0.001.

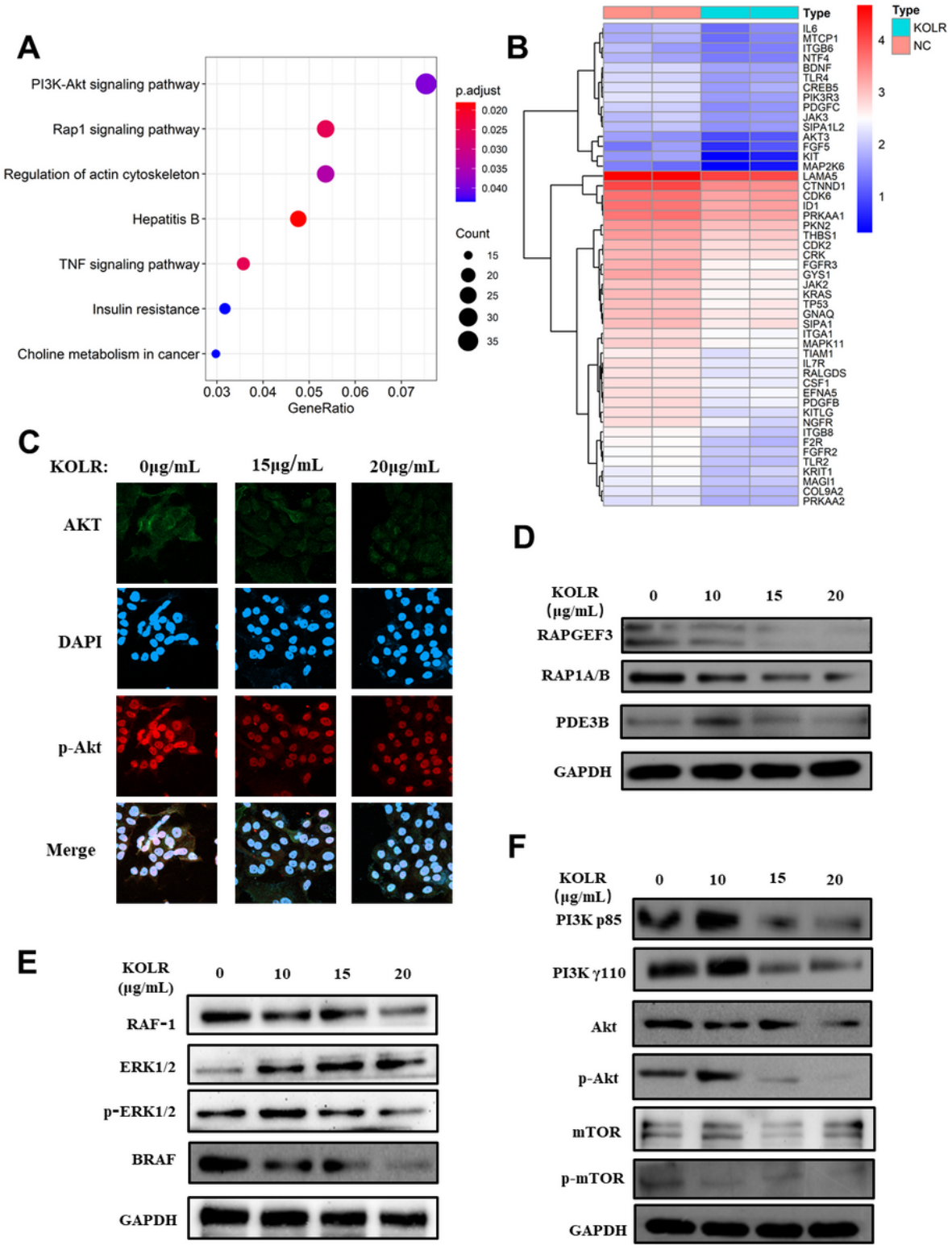

Figure 3

KOLR inhibits Rap-1 and PI3K-Akt signaling pathways. A. KEGG pathway analysis of down-regulated genes in BxCP-3 cells treated with KOLR. B. Heat map of downregulated genes of Rap-1 and PI3K-Akt signaling pathway. C. Confocal results of subcellular localization of Akt and p-Akt in BxCP-3 cells treated with different concentrations of KOLR. D. Immunoblots of RAPGEF3, RAP1A/1B, and PDE3B genes implicated in Rap-1 signaling pathway after treatment with different concentrations of KOLR. E. Protein

expression levels of ERK/BRAF signaling pathway factors such as BRAF, RAF1, ERK1/2, and Perk1/2 as determined by western blotting assays after treatment with different concentrations of KOLR. F. Immunoblots of PI3K p84, PI3K γ110, Akt, and p-Akt genes involved in PI3K/Akt signaling pathway after treatment with different concentrations of KOLR.

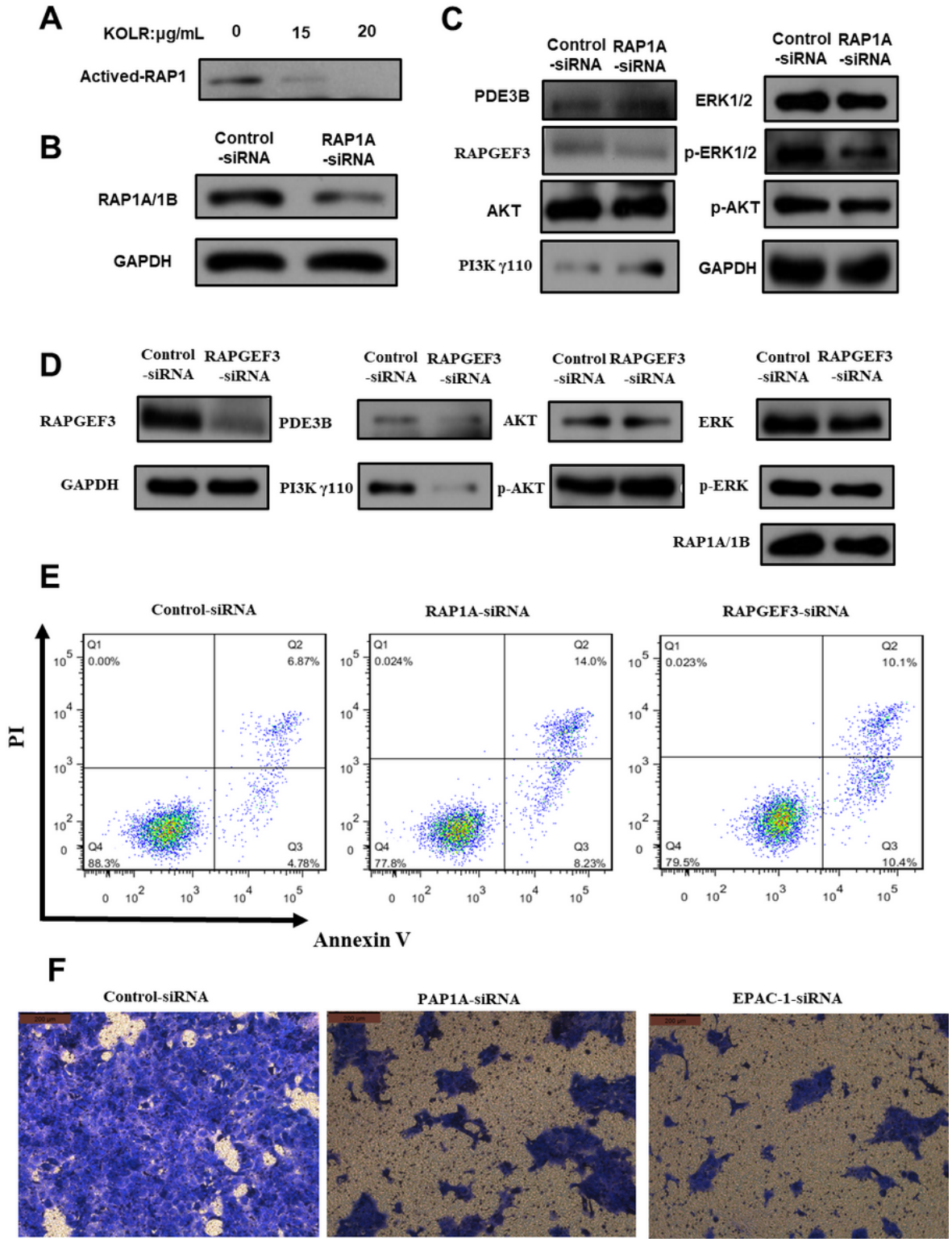

Figure 4

RAPGEF3 and RAP1A promote BxPC-3 cell migration and inhibit BxPC-3 cell apoptosis. A. KOLR inhibits activation of Rap-1 in a dose-dependent manner in BxPC-3 cells. B. RAP1A-siRNA knocked down the expression level of RAP1A/B. C. Expression levels of related genes of ERK1/2 and PI3K/Akt signaling pathway after RAP1A-siRNA knockdown. D. Expression levels of related genes of ERK1/2 and PI3K/Akt signaling pathway after RAPGEF3-siRNA knockdown. E. Apoptosis of BxPC-3 cells was activated after RAPGEF3 and RAP1A knockdown by siRNA. F. Invasion ability of BxCP-3 cells was inhibited after RAPGEF3 and RAP1A knockdown by siRNA.

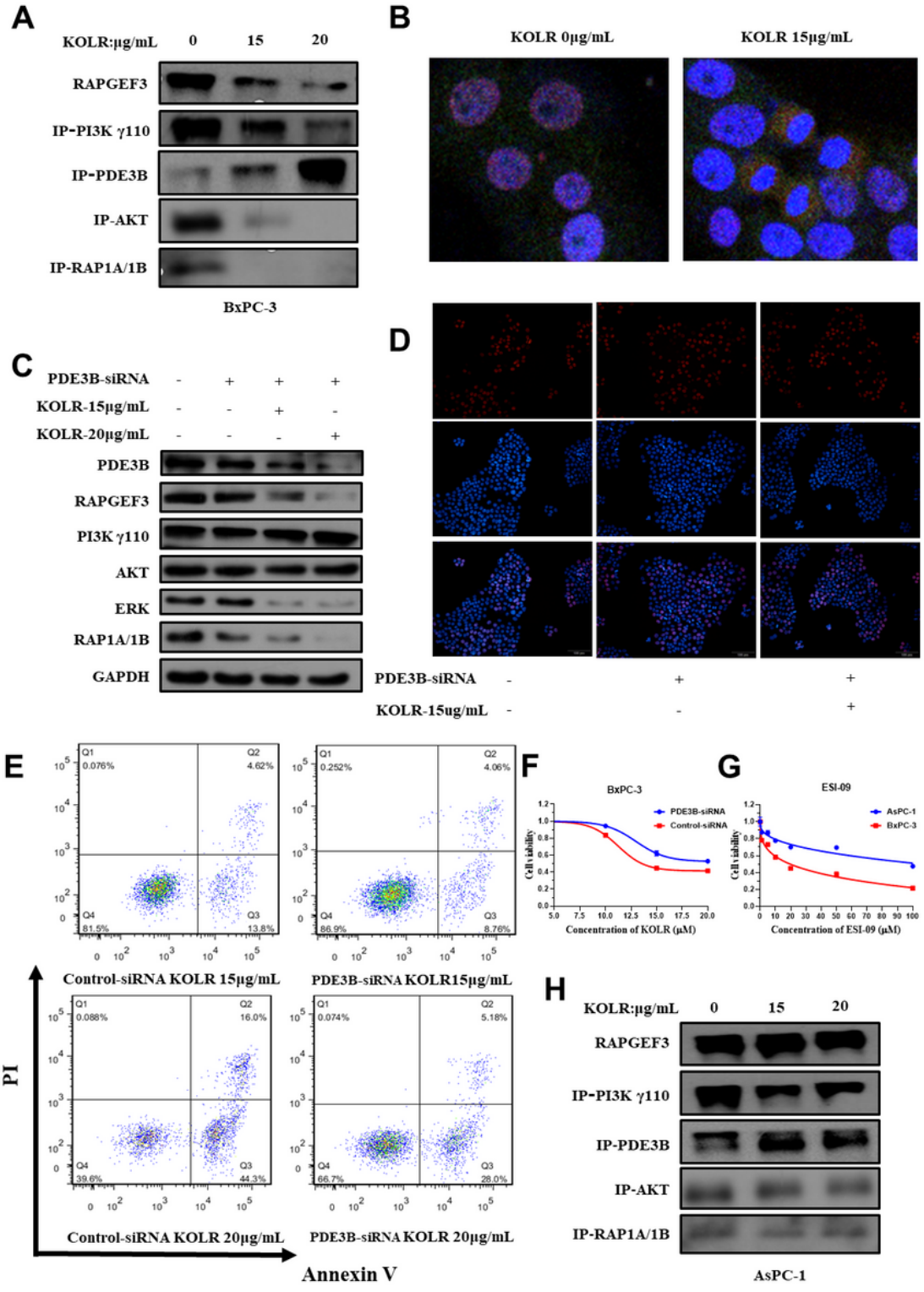

Figure 5

KOLR targets RAPGEF3/PDE3B complex and promotes complex formation to induce apoptosis of BxPC-3 cells. A. Immunoblots of RAPGEF3 binding proteins subjected to anti-RAPGEF3 immunoprecipitations in BxCP-3 cells. B. Confocal results of subcellular localization of RAPGEF3 and PDE3B in BxCP-3 cells treated with KOLR. C. Immunoblots of genes of Rap-1 and PI3K-Akt signaling pathway in BxCP-3 cells treated with KOLR after PDE3B-siRNA knockdown. D. Proliferation of BxPC-3 did not show significant difference after KOLR treatment after PDE3B-siRNA knockdown using the EDU assay. E. KOLR induced apoptosis of BxPC-3 cells was inhibited after knockout of PDBE3B. F. Resistance to KOLR of BxPC-3 cells was enhanced after knockout of PDBE3B. G. AsPC-1 cells were less sensitive to RAPGEF3 inhibitor ESI-09 compared with BxPC3 cells. H. Immunoblots of RAPGEF3 binding proteins subjected to anti-RAPGEF3 immunoprecipitations in AsPC-1 cells.

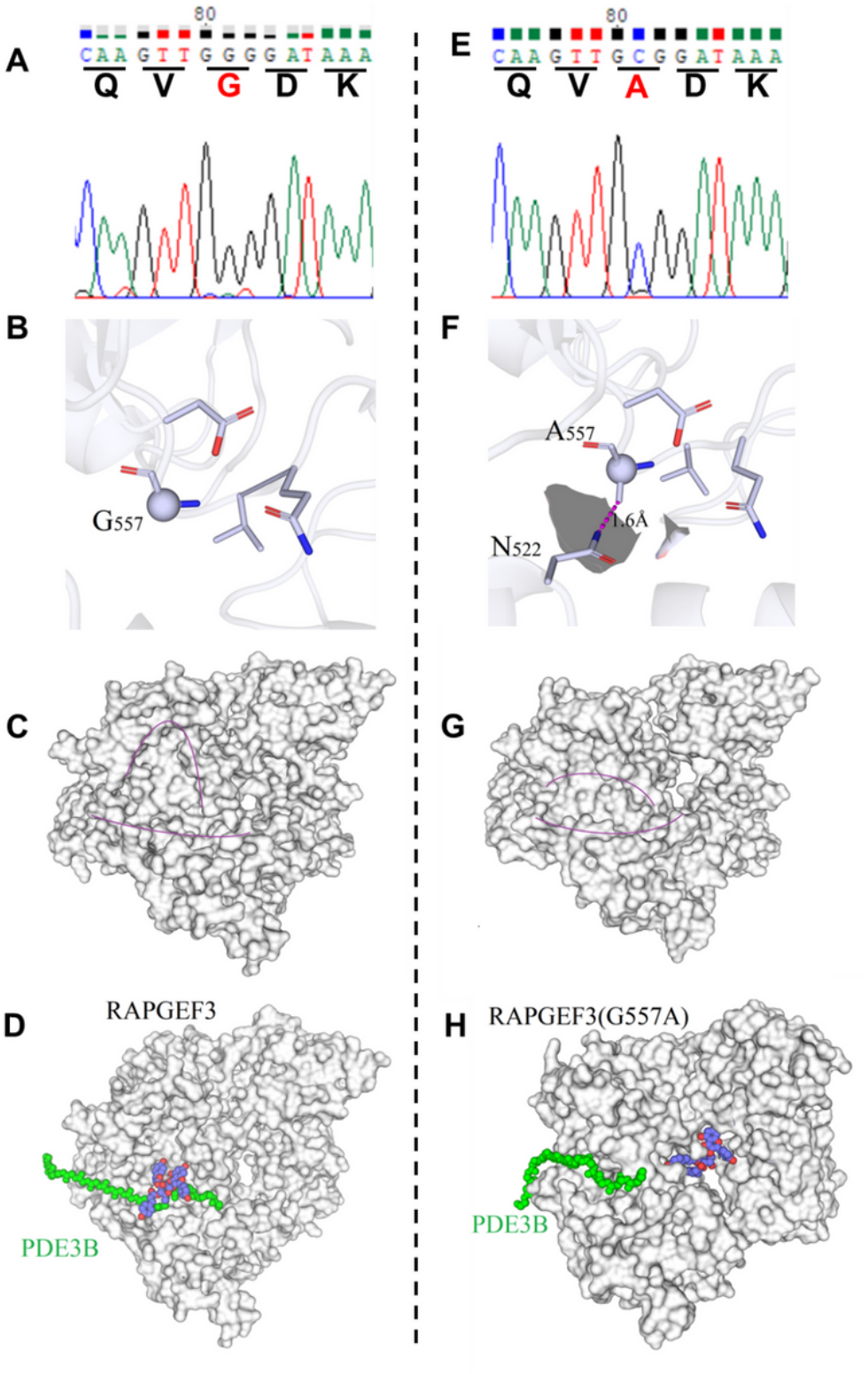

Figure 6

G557A mutation of RAPGEF3 affects formation of complexes. A. Mutation rates of RAPGEF3 in AsPC-1 and BxPC-3 cell lines. B. Physical-chemical reaction force and steric hindrance of RAPGEF3 WT and RAPGEF3 G557A. C. Average structure of RAPGEF3 (G557) and the mutant RAPGEF3 (A557) changed significantly at the binding site of PDE3B and KOLR. D. Binding structures of RAPGEF/PDE3B/KOLR complex for wild and mutant RAPGEF3.

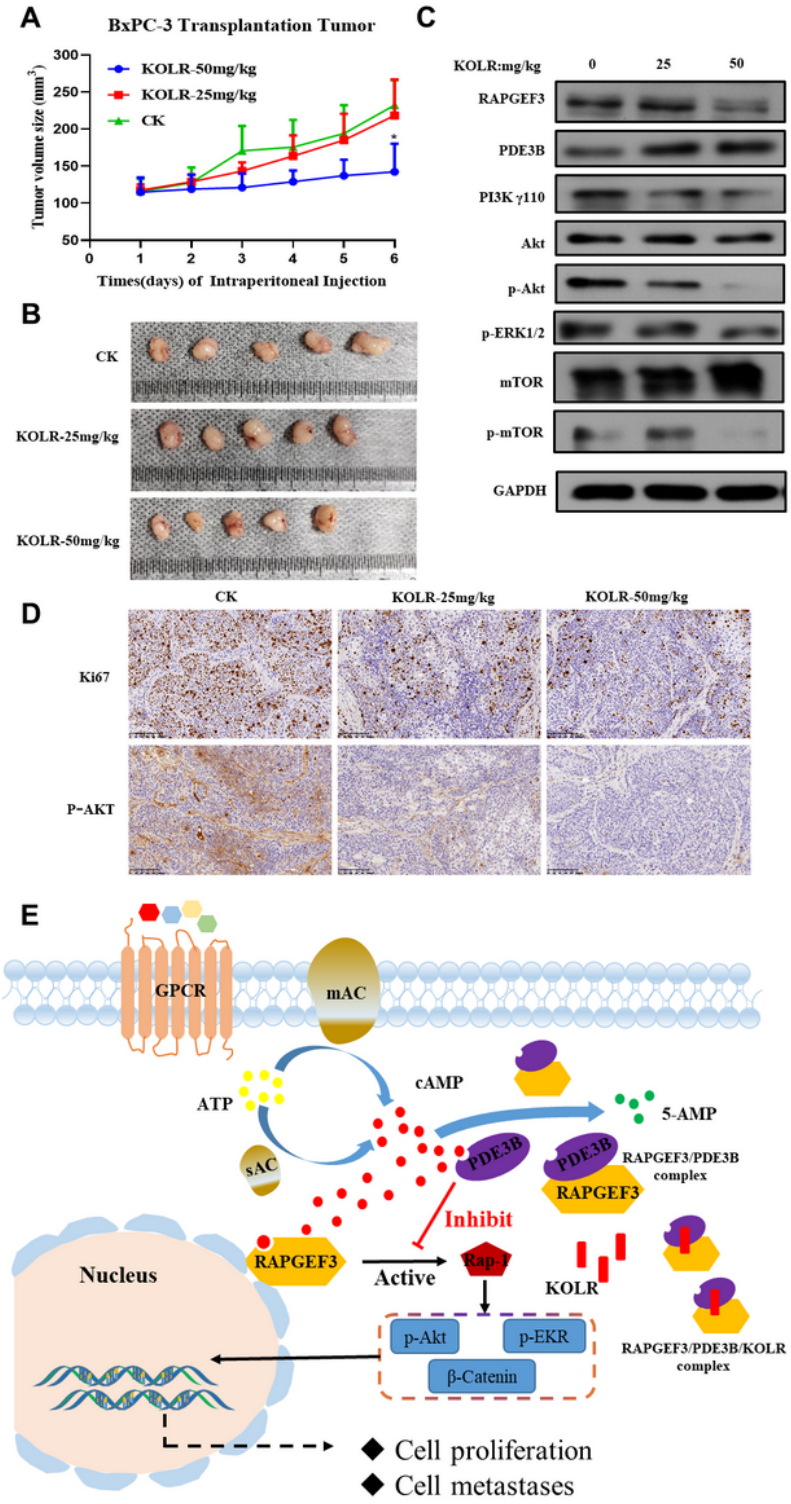

Figure 7

Anticancer effect and mechanism of KOLR in vivo. A. Tumor sizes during KOLR treatment. B. Images of nude mice tumors. C. Immunoblots of RAPGEF3, RAP1A/1B, and PDE3B genes of Rap-1 signaling pathway in tumor tissues after treatment with different concentrations of KOLR in vivo. D. IHC of Ki67 and p-Akt in tumor tissues after treatment with different concentrations of KOLR in vivo. E. Potential antitumor mechanisms of KOLR.

Supplementary Files

This is a list of supplementary files associated with this preprint. Click to download.

- SupplementaryTables.docx